Acta Crystallographica Section D
Biological Crystallography
ISSN 0907-4449

Structure of laminin-binding adhesin (Lmb) from *Streptococcus agalactiae*

Preethi Ragunathan,[a] Barbara Spellerberg[b] and Karthe Ponnuraj[a]*

[a]Centre of Advanced Study in Crystallography and Biophysics, University of Madras, Guindy Campus, Chennai 600 025, India, and [b]Institute of Medical Microbiology and Hygiene, University of Ulm, Ulm, Germany

Correspondence e-mail: pkarthe@hotmail.com

Received 30 July 2009
Accepted 22 September 2009

PDB Reference: laminin-binding adhesin, 3hjt, 3rhjtsf.

Adhesion/invasion of pathogenic bacteria is a critical step in infection and is mediated by surface-exposed proteins termed adhesins. The crystal structure of recombinant Lmb, a laminin-binding adhesin from *Streptococcus agalactiae*, has been determined at 2.5 Å resolution. Based on sequence and structural homology, Lmb was placed into the cluster 9 family of the ABC (ATP-binding cassette) transport system. The structural organization of Lmb closely resembles that of ABC-type solute-binding proteins (SBPs), in which two structurally related globular domains interact with each other to form a metal-binding cavity at the interface. The bound zinc in Lmb is tetrahedrally coordinated by three histidines and a glutamate from both domains. A comparison of Lmb with other metal transporters revealed an interesting feature of the dimerization of molecules in the crystallographic asymmetric unit in all zinc-binding transporters. A closer comparison of Lmb with the zinc-binding ZnuA from *Escherichia coli* and *Synechocystis* 6803 suggested that Lmb might undergo a unique structural rearrangement upon metal binding and release. The crystal structure of Lmb provides an impetus for further investigations into the molecular basis of laminin binding by human pathogens. Being ubiquitous in all serotypes of group B streptococcus (GBS), the structure of Lmb may direct the development of an efficient vaccine.

1. Introduction

Streptococcus agalactiae (group B streptococcus; GBS) is one of the most important neonatal pathogens, causing septicaemia and meningitis. It is commonly found in the maternal gastrointestinal and genitourinary tracts. Following peripartal transmission from mother to child, *S. agalactiae* is the predominant cause of invasive bacterial disease in neonates (Farley, 1995).

The adhesion of bacterial pathogens to host tissues is a critical early step in the process of infection. Numerous pathogenic bacteria adhere to host cells through surface proteins, termed adhesins, that bind to components of the extracellular matrix (ECM). The ECM of mammalian tissues consists of glycoproteins, including collagen, laminin, fibronectin and fibrinogen, and forms the macromolecular structure underlying the basement membrane of epithelial and endothelial cells (Ljungh & Wadstrom, 1995; Hay, 1991).

Several studies have demonstrated the ability of *S. agalactiae* to interact with ECM components such as fibronectin, fibrinogen and laminin and its implications in host-tissue adhesion and invasion (Broughton & Baker, 1983). Lmb, a 34 kDa surface-exposed lipoprotein from *S. agalactiae*

(UniProt Q9ZHG8), mediates the adherence of GBS to laminin (Jones *et al.*, 2000). Isogenic mutants of the *lmb* locus show substantially diminished adherence to immobilized laminin and the pre-incubation of immobilized laminin with recombinant Lmb significantly reduced the adherence of the wild type to laminin (Spellerberg *et al.*, 1999). These results indicate that Lmb may be essential for bacterial colonization of damaged epithelium and the translocation of bacteria into the bloodstream.

Laminin is a 900 kDa glycoprotein and forms a major component of the basement membrane. It is composed of three distinct polypeptide chains (A, B1 and B2) which reversibly assemble to form the macromolecular structure (Beck *et al.*, 1990). The adhesion of GBS to laminin may be critical for bacterial migration through the basal lamina and the interaction of Lmb with laminin could be a critical mechanism in this context. However, the structural basis of laminin binding is still unknown.

Transition metals, including iron, zinc, manganese, nickel and copper, participate in many structural and catalytic functions and are essential for the pathogenesis of infections. However, these metals may also participate in destructive metal-based reactions at high concentrations (Finney & O'Halloran, 2003). Thus, to be pathogenic the bacteria must evolve mechanisms to control the influx and efflux of metals within the bacterial cell, as it is constantly exposed to fluctuating levels of transition metals in the host environment (Weston *et al.*, 2009).

Previous analysis of the gene sequence of Lmb shows that it exhibits significant homology to the LraI (lipoprotein receptor antigen) protein family (Spellerberg *et al.*, 1999), members of which are known to play varied roles as adhesins, virulence factors and transport proteins in many bacteria (Dintilhac *et al.*, 1997). The majority of these transporter proteins belong to the ATP-binding cassette (ABC) superfamily of transport systems, which typically represent 40% of the putative lipoproteins in Gram-positive bacteria (Hutchings *et al.*, 2008). The ABC-type transporters or solute-binding proteins (SBPs) have been classified into at least nine subfamilies, reflecting the broad range of substrates transported, and make a vital contribution to the ability of prokaryotes to acquire diverse substrates from their environments (Claverys, 2001; Lawrence *et al.*, 1998). These substrates include sugars, siderophores, divalent metal ions, anions (such as phosphate and sulfate), amino acids, oligopeptides and nucleosides (Hutchings *et al.*, 2008). Phylogenetic analysis and sequence homology placed Lmb as a solute-binding protein in the cluster 9 family of ABC-type metal-binding proteins, which includes zinc-specific and manganese-specific transporters. However, the typical ATP-binding cassette or transmembrane regions of bacterial ABC transporters have so far not been found in the genetic locus encoding the *lmb* gene.

Structural information is currently available for seven metal transporters of the cluster 9 family: the Zn^{2+}-bound PsaA (Lawrence *et al.*, 1998) and AdcAII (Loisel *et al.*, 2008) from *S. pneumoniae*, ZnuA from *Escherichia coli* (ZnuA-Ec; Li & Jogl, 2007; Chandra *et al.*, 2007), ZnuA from *Synechocystis* 6803 (ZnuA-Syn; Banerjee *et al.*, 2003) and TroA from *Treponema pallidum* (Lee *et al.*, 1999) and the Mn^{2+}-bound MntC from *Synechocystis* 6803 (Rukhman *et al.*, 2005) and the more recent structurally characterized Lbp from *S. pyogenes* (Linke *et al.*, 2009). The structures of TroA (Lee *et al.*, 2002) and ZnuA-Syn (Wei *et al.*, 2007) have also been determined in the metal-free state. Although the overall topology and bilobed structure is conserved in all these structures, significant variations are observed in the metal-binding site and the nearby loop regions. Here, we report the crystal structure of Lmb at 2.5 Å resolution. Structural analysis of Lmb has provided new leads for further investigations into the molecular basis of laminin binding by GBS. The ubiquitous nature of Lmb in all serotypes of *S. agalactiae* makes it an attractive target for a GBS vaccine.

2. Materials and methods

2.1. Cloning, expression and purification of Lmb

The cloning, expression, purification and crystallization of Lmb have been described previously (Spellerberg *et al.*, 1999; Ragunathan *et al.*, 2009). In brief, the *lmb* gene spanning residues 19–305 was cloned into pET21a expression vector (Novagen, Madison, Wisconsin, USA) containing a C-terminal 6×His tag and overexpressed in *E. coli* BL21 (DE3) (Novagen). Lmb was purified by immobilized metal-affinity chromatography (IMAC) using Ni–NTA matrix and a buffer consisting of 20 m*M* Tris pH 7.0, 300 m*M* NaCl, 0.1% Triton X-100, 5% glycerol and 5 m*M* β-mercaptoethanol with a linear gradient of imidazole from 20 to 250 m*M*. Fractions containing greater than 80% homogenous protein, as observed by SDS–PAGE, were pooled and concentrated and buffer exchange was carried out using an Amicon concentrator (Centriprep) to remove the imidazole. The protein was further purified by gel filtration using a Sephadex S-75 column (GE Biosciences) and eluted with buffer containing 20 m*M* Tris pH 7.0, 300 m*M* NaCl, 0.1% Triton X-100, 5% glycerol and 5 m*M* β-mercaptoethanol. The fractions corresponding to Lmb were pooled and concentrated. The concentration of the protein was determined from the A_{280} as measured using a UV spectrophotometer and the yield of protein was found to be 35 mg per litre of culture.

2.2. Crystallization

Crystallization of Lmb was carried out by the hanging-drop vapour-diffusion method at 293 K by mixing equal volumes (1 µl) of protein and reservoir solutions. The drop was equilibrated against 1 ml reservoir solution containing 30% PEG 2000 monomethyl ether as precipitant. Thin plate-like crystals grew within 3 d. The quality of the crystal was improved after a series of crystallization trials with various additives such as divalent metal ions, glycerol and ethylene glycol. Crystals for crystallographic studies were obtained with 30–35%(*w*/*v*) PEG 2000 monoethyl ether, 0.1 m*M* sodium citrate pH 5.0, 5 m*M* $NiCl_2$ and 10% ethylene glycol.

Table 1
Statistics of diffraction data collection and structure refinement.

Values in parentheses are for the highest resolution shell.

Crystal parameters	
Space group	$P2_1$
Unit-cell parameters (Å, °)	a = 56.63, b = 70.60, c = 75.37, β = 96.8
Z' (molecules per ASU)	2
Matthews coefficient (Å^3 Da^{-1})	2.2
Solvent content (%)	44
Data-processing statistics	
Temperature of measurement (K)	100
Wavelength (Å)	1.5418
Resolution (Å)	20–2.5 (2.59–2.50)
Total reflections	75211
Unique reflections	19066
Completeness (%)	98.7 (99.9)
$R_{\rm merge}$ (%)	5.4 (27.4)
Mean $I/\sigma(I)$	5.6 (1.4)
Refinement statistics	
Resolution range (Å)	20–2.5
$R_{\rm work}/R_{\rm free}$† (%) (all data with 0$\sigma$ cutoff)	23.3/27.5
No. of non-H protein atoms	4066
No. of water molecules	95
No. of Zn^{2+} ions	2
Root-mean-square deviations	
Bond lengths (Å)	0.009
Bond angles (°)	1.569
Average B factor (Å^2)	
All protein atoms	55.4
Metal ions	40.1
Waters	49.4
Ramachandran plot (%)	
Most favoured	90.0
Additional allowed	9.8
Generously allowed	0.2
Disallowed	0.0
PDB code	3hjt

† $R_{\rm free}$ used a random 5% reserve of the working set of reflections.

2.3. Data collection and processing

For X-ray data collection, Lmb crystals were flash-cooled in a nitrogen-gas stream at 100 K. Diffraction data were collected at our in-house data-collection facility using a MAR345 image-plate detector and a Bruker Microstar copper rotating-anode generator operating at 60 mA and 45 kV. A total of 100 frames were collected with an oscillation step of 1.5° and an exposure of 300 s per frame. Diffraction images were indexed, integrated, merged and scaled using the *AUTOMAR* software package (Bartels & Klein, 2003). The data-collection statistics are summarized in Table 1.

2.4. Structure determination

The structure of Lmb was solved by molecular replacement using the program *CNS* (Brünger *et al.*, 1998) and also using the online server *BALBES* (Long *et al.*, 2008). The homology model of Lmb was generated using the monomer of its closest homologue of known structure, AdcAII from *S. pneumoniae* (Loisel *et al.*, 2008; PDB code 3cx3), and was used as a search model for the initial structure determination. A rotation and translation search identified two monomers in the asymmetric unit. After rigid-body refinement (resolution range 20–2.5 Å, R factor of 45.8%), the noncrystallographic symmetry (NCS) matrix was evaluated. The model was subjected to simulated annealing and iterative cycles of positional and temperature-factor refinement (20–2.5 Å) followed by manual fitting and rebuilding. Atomic refinement of the model was performed using the program *CNS* with tight NCS restraints using a force constant of 1256 kJ mol^{-1} Å^{-2} (Brünger *et al.*, 1998). The program *Coot* (Emsley & Cowtan, 2004) was used for model building and also for assigning water molecules.

The final model was established after many cycles of manual rebuilding followed by refinement and had an R factor of 23.3% and an $R_{\rm free}$ of 27.5% (all data with 0σ cutoff). This model contained three disordered regions in both molecules *A* (residues 19–31, 100–104 and 123–137) and *B* (residues 19–31, 100–104 and 122–138). The side-chain densities for some residues (Asp99, Lys104, Lys106, Thr137, Lys167, Ser199, Lys200 and Asp257 in molecule *A*, and Lys104, Ser105 and Lys106 in molecule *B*) were not clear and therefore side-chain atoms were not included beyond the C$^\beta$ atom for these residues. The refinement statistics are summarized in Table 1.

3. Results and discussion

3.1. Sequence analysis of Lmb

A *BLAST* (Altschul *et al.*, 1997) analysis of the Lmb sequence against the nonredundant protein database identified several homologues with sequence identities ranging from 99 to 25%, the majority of which have been identified as laminin-binding surface proteins from various Gram-positive and Gram-negative bacteria. The homologues that have been annotated include laminin-binding proteins from *S. pyogenes* (99% sequence identity), *S. equisimilis* (95%) and *S. dysgalactiae* subsp. *equisimilis* (99%), zinc-binding lipoprotein AdcA from *S. pneumoniae* (65%), adhesion lipoprotein from *S. pneumoniae* (65%), Zn porter lipoprotein from *S. sanguis* (61%) and metal-binding lipoprotein from *S. gordonii* (58%). A comparison of these sequences revealed that nearly 38% of residues (115 of 305) are highly conserved in all these proteins.

It is interesting to observe that a high degree of sequence conservation is seen in the N-terminal region compared with the C-terminal region. The residue Cys19 that forms a part of the signal peptide, which is assumed to undergo covalent attachment to a diacylglycerol moiety followed by proteolytic cleavage (Spellerberg *et al.*, 1999), is also conserved in all the homologues. This suggests that all these proteins are translocated and secreted in a similar fashion. Another notable feature observed is that the majority of the residues conserved are hydrophobic, such as Met33, Val35, Phe39, Ile59, Val107 and Leu118. While most of the solute-binding proteins are considered to be remarkably hydrophilic molecules (Boos & Lucht, 1995), mutational studies suggest that several hydrophobic amino acids are directly involved in interaction with membrane transport components (Shilton *et al.*, 1996). These amino acids might constitute hydrophobic patches that are responsible for a nonspecific and strong interaction between solute-binding proteins (SBPs) and the transport components or among SBPs themselves during oligomerization. In addition, the residues His66, His142, His206 and Glu281 that form

the metal-binding site in Lmb are also highly conserved in all these species. The DPH motif (140–142), containing the metal-binding histidine residue, is strictly conserved, suggesting that all the homologues of Lmb might follow a similar mode of metal binding.

3.2. Overall structure

Lmb (19–305; 287 residues) has been crystallized in a monoclinic space group with two crystallographically independent molecules in the asymmetric unit. The final model consisted of molecule *A* with 260 residues, molecule *B* with 257 residues, two metal ions (one per molecule) and 95 water molecules. The two molecules are isomorphous and superimpose with a root-mean-square (r.m.s.) deviation of 0.38 Å between all 257 corresponding C^{α} atoms. Each monomer is made up of two independent domains, an N-terminal domain (residues 31–167) and a C-terminal domain (197–305), that are related by twofold pseudosymmetry (Fig. 1). Despite having low sequence identity (15.4%), the two domains share the classic β/α topology consisting of a four-stranded parallel β-sheet flanked by α-helices and superimpose with an r.m.s. deviation of 3 Å for 121 C^{α} atoms. The interface between the two domains has a narrow and deep cavity in which the metal ion binds. The metal ion is well buried in this cavity with very little accessibility to the solvent. There are very few direct interactions that occur between the two domains and the metal ion interacts with residues from both domains and appears to hold the domains intact.

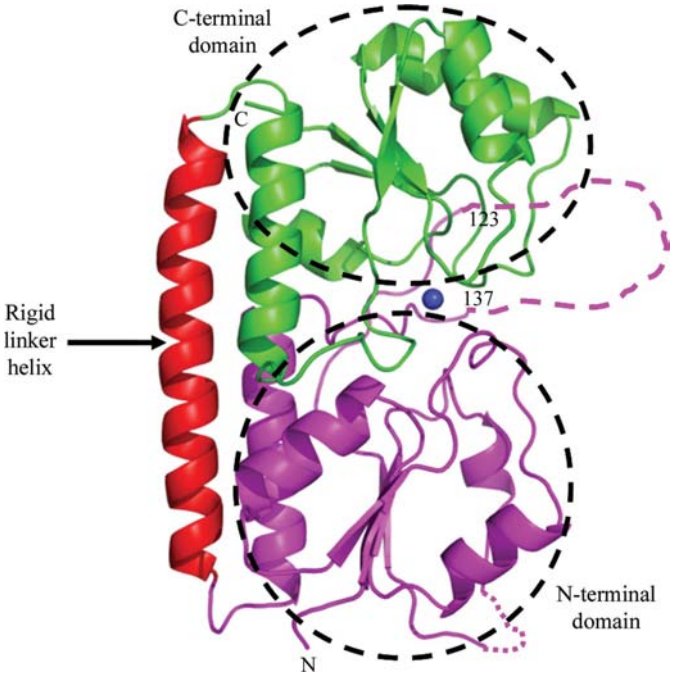

Figure 1
Overall structure of Lmb. The molecule contains two domains: the N-terminal domain (magenta) and the C-terminal domain (green). The linker helix that joins these two domains is indicated in red. The blue sphere represents the bound metal ion which is located in the interdomain interface. The missing loop region (123–137) in the metal-binding site is shown in magenta dotted lines.

The two domains are connected by a 'rigid linker helix' formed by residues 169–197 which acts as a backbone and runs almost the entire length of the protein, analogous to those observed in other metal-binding proteins (Lawrence *et al.*, 1998; Banerjee *et al.*, 2003; Li & Jogl, 2007; Loisel *et al.*, 2008; Fig. 1). The crystal structures of SBPs that transport large solutes, such as maltose- or maltodextrin-binding protein (Sharff *et al.*, 1992), L-arabinose-binding protein (ABP; Newcomer *et al.*, 1981) and leucine/isoleucine/valine-binding protein (Sack *et al.*, 1989), reveal the presence of two or three flexible β-strands that connect the N- and C-terminal domains. These β-strands act as a hinge for the opening and closure of the two domains and thereby alter the conformation of the ligand-binding pocket at the interdomain cleft for substrate exchange. A comparison of the crystal structures of SBPs that transport large solutes with those of metal transporters show that although the overall bilobed structure is conserved, significant differences are observed in the topology of the secondary-structural elements. Most importantly, the interdomain linker, the flexible β hinge observed in the SBPs transporting large solutes, is replaced by a rigid helix in Lmb and in other metal transporters, leading to a more constrained interdomain opening upon metal binding in these structures.

At the N-terminus, the first 19–31 residues that follow the signal peptide cleavage site are not very well defined in Lmb, as in PsaA (Lawrence *et al.*, 1998) and ZnuA-Syn (Banerjee *et al.*, 2003). There is no interpretable electron density for these residues and hence it is probable that this region does not interact with the core elements of the N-terminal domain. In addition, sequence comparison shows that this region seems to be the least conserved in most of the metal-binding transporters for which structures have been solved to date. This is not surprising considering that this region is made up predominantly of hydrophobic residues and is likely to be a flexible tether connecting the metal-binding domain to the membrane anchor, bridging the protein and lipid surface in the cell.

3.3. Metal-binding site

The metal-binding site in Lmb, as identified by a strong $F_o - F_c$ electron-density peak, is located in the cleft at the interface between the N- and C-terminal domains (Fig. 1). The metal ion is tetrahedrally coordinated by three histidines (His66, His142 and His206) *via* their $N^{\varepsilon 2}$ atoms and one glutamate (Glu281) *via* its $O^{\varepsilon 2}$ atom. The coordinating distances between the metal ion and the amino-acid atoms are 2.13 Å to His66 $N^{\varepsilon 2}$, 2.33 Å to His142 $N^{\varepsilon 2}$, 2.19 Å to His206 $N^{\varepsilon 2}$ and 2.18 Å to Glu281 $O^{\varepsilon 2}$ (Fig. 2). This tetrahedral coordination is a common feature of Zn^{2+}-binding proteins (Rulísek & Vondrásek, 1998). Furthermore, in Lmb the mean distances between the metal ion and the electron donors are in close agreement with the distances observed for the Zn^{2+} ion. It is likely that this Zn^{2+} was acquired from traces of the metal in the buffers used during expression and purification of the protein, despite the protein being crystallized with Ni^{2+}, which prefers to form an octahedral coordination (Rulísek &

Vondrásek, 1998). In Lmb, the metal-binding pocket is formed by two residues each from both the N-terminal and C-terminal domains, analogous to AdcAII (Loisel *et al.*, 2008), PsaA (Lawrence *et al.*, 1998), TroA (Lee *et al.*, 1999) and MntC (Rukhman *et al.*, 2005) and in contrast to ZnuA-Ec (Li & Jogl, 2007) and ZnuA-Syn (Banerjee *et al.*, 2003), where the C-terminal domain contributes only one residue to the active site or to Zn^{2+} coordination. The residues in the second coordination shell of the metal ion are Asp140, Ser227 and Glu255, and interact with the active-site histidines as shown in Fig. 2. The two monomers of Lmb show identical geometry at the metal-binding site in addition to a high degree of similarity in all the loop regions.

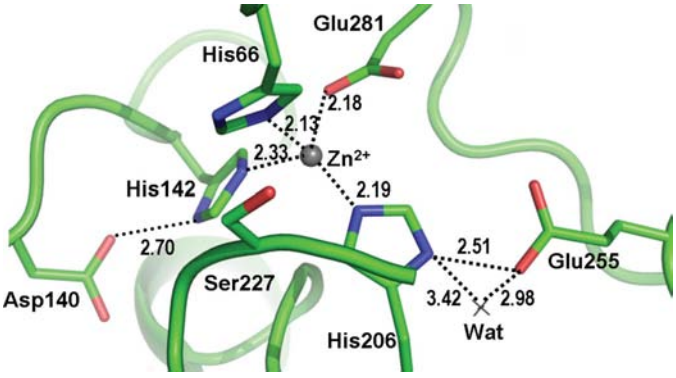

Figure 2
Metal-binding site in Lmb. The grey sphere shows the bound zinc ion that is tetrahedrally coordinated to His66, His142, His206 and Glu281. The second-shell coordination residues Asp140, Ser227 and Glu255 are also indicated.

3.4. Structure comparison of Lmb with other ABC-type SBPs

Proteins with a structure homologous to Lmb were identified by a *DALI* (Holm *et al.*, 2008) search. The two closest homologues identified were the zinc-binding protein AdcAII from *S. pneumonia* (PDB code 3cx3) and the manganese transporter protein MntC from *Synechocystis* 6803 (PDB code 1xvl), with *Z* scores of 37 and 36, respectively. Other close

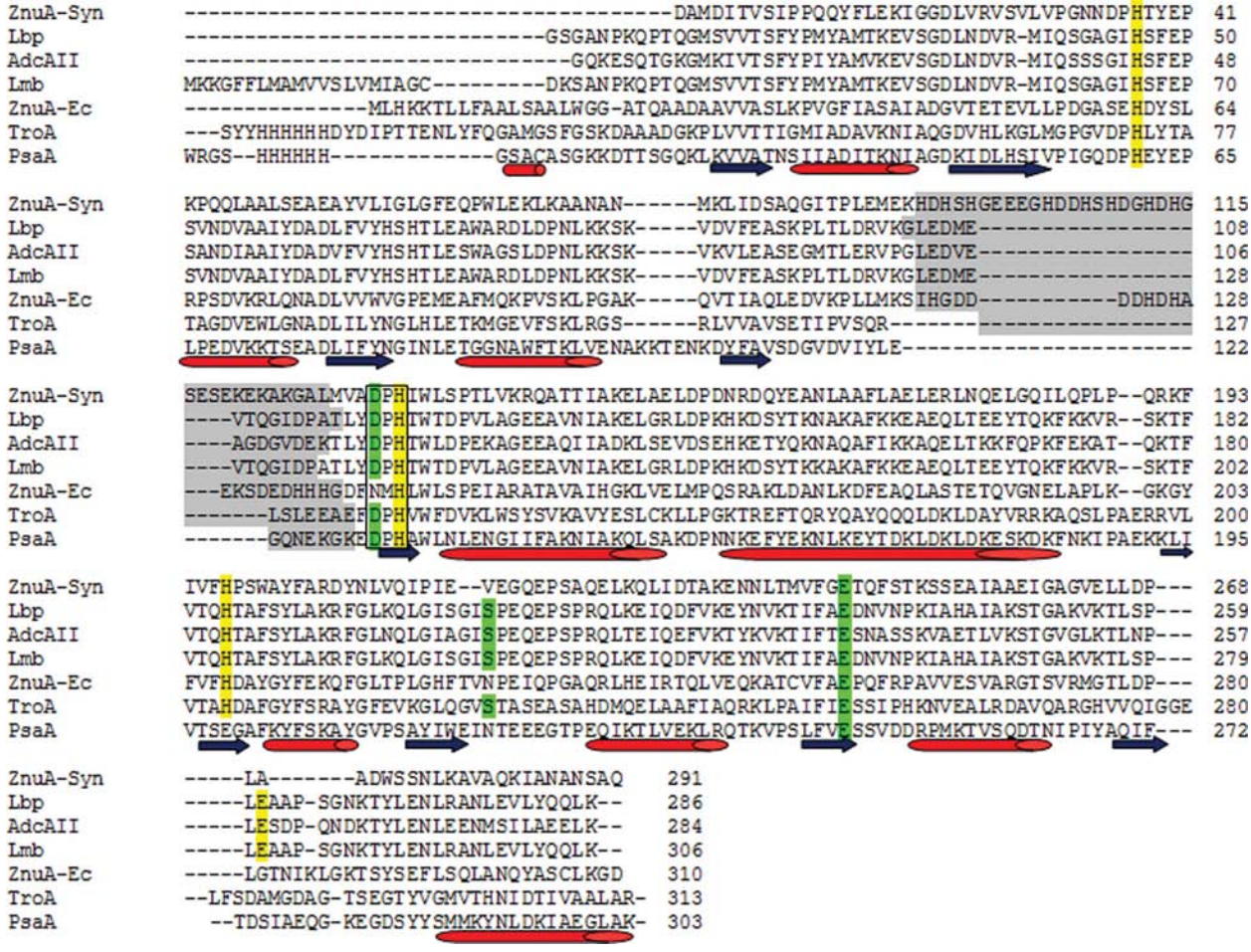

Figure 3
Structure-based sequence alignment of Lmb with other metal-binding SBPs from the ABC-cluster 9 family of proteins. The percentage sequence identity of Lmb with its homologues is also indicated. ZnuA-Syn (*Synechocystis* 6803, 24.23%), Lbp (*S. pyogenes*, 94.44%), ZnuA-Ec (*E. coli*, 20.99%), TroA (*T. pallidum*, 22.97%), AdcAII and PsaA (*S. pneumonia*, 66.12 and 31.43%, respectively) are used for comparison. The DPH motif and metal-binding residues are highlighted in yellow. The secondary-shell residues are highlighted in green and the residues that form the metal-binding loop are indicated in grey. The blocks represent α-helix and arrows represent β-strand.

Table 2
Sequence information for the metal-binding loop in various Zn^{2+}-binding SBPs.

Protein	PDB code	Loop sequence (residue range)	Ordered/disordered in the structure
Lmb	3hjt	LEDMEVTQGIDP (124–135)	Disordered
Lbp	3gi1	GLEDMEVTQGIDPAT (123–137)	Disordered
ZnuA-Syn	1pq4	HDHSHGEEEGHDDHSHDGHDHGSESEKEKAKGAL (140–173)	Disordered
ZnuA-Ec	2ogw	IHGDDDDHDHAEKSDEDHHHG (136–157)	Disordered
AdcAII	3cx3	LEDVEAGDGVDEK (129–142)	Disordered
PsaA	1psz	GQNEKGK (129–135)	Ordered
TroA	1toa	EEAE (126–129)	Ordered

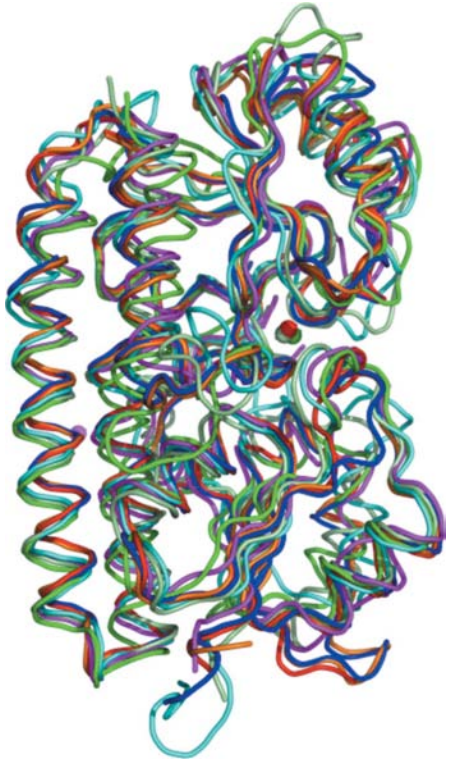

Figure 4
Structural alignment of Lmb with other zinc-binding SBPs. Ribbon diagram of the superimposed structures of Lmb (red) with AdcAII (PDB code 3cx3, blue, r.m.s.d. 0.929 Å), PsaA (1psz, cyan, r.m.s.d. 1.563 Å), ZnuA-Ec (2osv, green, r.m.s.d. 1.842 Å), TroA (1toa, pale green, r.m.s.d. 1.606 Å), ZnuA-Syn (1pq4, magenta, r.m.s.d. 1.987 Å) and Lbp (3gi1, orange, r.m.s.d. 0.542 Å). The metal ions are indicated by a coloured sphere.

homologues of Lmb are the periplasmic binding protein TroA from *T. pallidum* (PDB code 1toa; *Z* score 29.9), the pneumococcal surface antigen PsaA from *S. pneumonia* (PDB code 1psz; *Z* score 29.4), the Zn transporter ZnuA from *Synechocystis* (PDB code 1pq4; *Z* score 28.8) and metal transporter proteins from various other species. During the review of this manuscript, the structure of another very close homologue of Lmb, Lbp from *S. pyogenes*, has been published (PDB code 3gi1; Linke *et al.*, 2009). Lbp and Lmb show a very high degree of sequence as well as structural homology. A structure-based sequence alignment of Lmb and its homologues is presented in Fig. 3.

The superimposition of these structures shows that the positions of the secondary-structure elements remain conserved, while the majority of the loop regions, particularly those involved in metal binding, show significant variations in their backbone conformations (Fig. 4). The position of the metal ion and the geometry of the metal-binding site are similar in all the homologues of Lmb. However, subtle differences in the zinc-coordinating residues are observed. For example, His206 in Lmb is replaced by Glu205 at a homologous position in PsaA and Glu281 of Lmb is replaced by Asp280 and Asp279 in PsaA and TroA, respectively.

In all the zinc-binding SBPs, it is believed that a flexible loop region in the active site functions as a metal-binding chaperone and increases the metal affinity of the transporter (Banerjee *et al.*, 2003). In addition, a deletion mutant of this loop region revealed that the loop may act as a sensor and plays a regulatory role in zinc transport (Wei *et al.*, 2007). In Lmb this loop (residues 123–137; Fig. 1) is disordered in the crystal structure and was therefore omitted from the final model. A similar disorder in the corresponding loop was observed in some of the metal-binding SBPs such as Lbp, AdcAII, ZnuA-Syn and ZnuA-Ec. It is commonly noted that this loop is of varying lengths in Zn^{2+} transporters. In some cases, such as ZnuA-Syn and ZnuA-Ec, it is highly charged and rich in histidines. The sequence information and variation of this metal-binding loop in various SBPs is given in Table 2. It is postulated that free zinc is at a low concentration in both the periplasm and cytoplasm and the charged loops in zinc transporters are important to sequester zinc to the metal-binding cleft (Banerjee *et al.*, 2003). Interestingly, this loop is relatively short and is not charged in Lmb.

3.5. Dimer assembly

Structural comparison of Lmb with other ABC-type SBPs provides the interesting observation that all the zinc-binding cluster 9 proteins exhibit a dimeric assembly of molecules in the crystallographic asymmetric unit. Nevertheless, the interactions across the dimer interface and the orientation of the monomers in the asymmetric unit are distinct in each of these structures (Supplementary Fig. S1[1]). It is an intriguing question whether all the zinc-binding SBPs exist as dimers in solution, as there are no reports of the oligomeric states of these proteins in solution. However, gel-filtration chromatography indicates that Lmb exists as a dimer in solution (data not shown). In the crystal structure of Lmb the dimer is loosely packed, with only 36 intermolecular contacts (<4 Å), while TroA is the most tightly packed with 163 contacts across the dimer. In Lmb only a small area of the surface of each

[1] Supplementary material has been deposited in the IUCr electronic archive (Reference: MV5030). Services for accessing this material are described at the back of the journal.

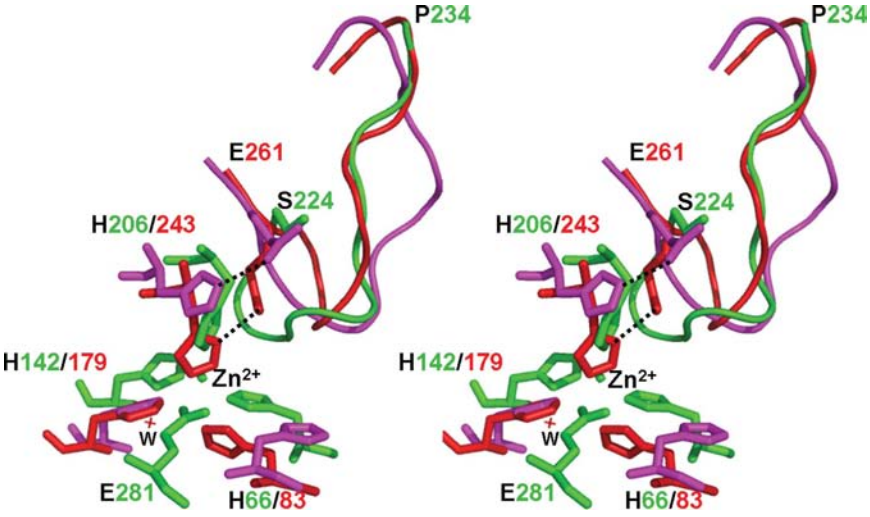

Figure 5
Stereoview of superposition of the active-site region of Lmb (green) with ZnuA-Syn (red, metal-bound; magenta, metal-free). The dotted line indicates the hydrogen bond.

monomer participates in monomer–monomer interactions, with 330 Å^2 of each monomer, or 3% of the entire surface of Lmb, buried upon dimer formation. This kind of dimer association is not observed in the crystal structure of Mn transporters within the cluster 9 family such as PsaA and MntC, making it a unique feature of Zn transporters. However, the dimeric association of molecules in the asymmetric unit could merely be a crystallographic artifact of little biological relevance. The physiological relevance of the dimeric assembly and its role in the function of the proteins, if any, needs to be elucidated.

3.6. Metal binding and release

The structural features described for Lmb reveal a high affinity of the protein for metal binding. It is observed that the interactions of the metal ion with the side-chain residues of the protein create a tightly packed structure which does not allow the metal ion to escape easily. Hence, the entry, binding and release of the bound metal necessitate a structural rearrangement of the protein.

In Lmb, the linker helix interacts with elements of both the N-terminal and C-terminal domains to form a well packed structure with a hydrophobic core, making it more rigid than the interdomain linker β-strands of the SBPs that transport large molecules. A comprehensive analysis of the metal-binding and large solute-binding SBPs reveals that the metal-binding clefts are narrower and deeper. The metal-binding environment and the N-terminal and C-terminal domain interface are hydrophilic in metal-binding transporters, while they are predominantly hydrophobic in the solute-binding counterparts depending on the nature of the molecules they transport. Also, the loops that surround the ligand-binding cavity are short in large solute-binding SBPs, making the cavity more open and wide for free movement of the large solutes, in contrast to the metal-binding loops, which are longer and of variable length. *In toto*, the solute-binding proteins that bind larger ligands utilize the Venus flytrap mechanism which is based on the movement of the linker β-strands between the N-terminal and C-terminal domains (Sack *et al.*, 1989) and is not applicable to the metal-binding SBPs.

To date, there has not been a clear understanding of the mode of metal transport in SBPs. A hypothetical mechanism known as 'partial domain slippage' for metal binding and release has been proposed based on the crystal structure of ZnuA-Ec (Chandra *et al.*, 2007). However, several of the structural features discussed for ZnuA-Ec are not observed in Lmb.

A close comparison of Lmb with ZnuA-Syn in the apo and the metal-bound form suggests that zinc is bound to the three active-site histidines in Lmb (His66, His142 and His206) analogous to the case in ZnuA. However, the fourth metal coordination in Lmb is provided by Glu255, which is replaced by water in ZnuA-Syn. In ZnuA, when zinc is released His243 and Glu261 move out of the metal-binding pocket, retaining their hydrogen bond. In Lmb, this Glu261 is replaced by Ser224 at an analogous position and a hydrogen bond is not observed between His206 and Ser224. Also, a loop region (Ser224–Pro234) in Lmb located at the mouth of the metal-binding cavity shows significant conformational differences compared with the corresponding loop in metal-bound and apo ZnuA-Syn. A stereoview of superposition of the active-site region of Lmb with apo and metal-bound ZnuA-Syn is shown in Fig. 5. Considering the structural differences that are observed between Lmb and ZnuA-Ec/ZnuA-Syn in the metal-binding site and nearby loop regions, it is likely that the residue-level structural change that would occur in Lmb when zinc is bound and released might be distinct from the structural variations observed for both ZnuA-Ec and ZnuA-Syn. Hence, we hypothesize that each metal-binding SBP might follow a unique mechanism of metal binding and release.

4. Conclusions

The structure of Lmb clarifies the ambiguous functional annotation of Lmb. From the crystal structure and the genomic location of the *lmb* gene, we believe that Lmb has a role in zinc homeostasis. In contrast, previous studies have shown *in vitro* binding of Lmb to laminin, confirming its function as an adhesin. Although the crystal structure of Lmb reveals a bound zinc ion, the genomic context of Lmb is different from other metal-binding proteins in the sense that it is not found in an operon that encodes an associated cognate permease, a regulator and an ATPase. In contrast, Lmb is encoded in an operon together with a protein that belongs to the family of streptococcal histidine triad proteins and is a zinc-binding protein (Kunitomo *et al.*, 2008), as in the cases of

Lbp and AdcAII. The co-transcription of two zinc-binding proteins such as Lmb and the histidine-triad protein suggests that this operon might be involved in zinc homeostasis.

Pathogenic microorganisms express cell-surface proteins that attach to mammalian ECM molecules. This interaction promotes bacterial colonization and infection of damaged tissues. Currently, structural information is available for surface proteins of Gram-positive bacteria that bind to collagen (Zong *et al.*, 2005), fibrinogen (Ponnuraj *et al.*, 2003) and fibronectin (Pilka *et al.*, 2006). Although the structure of Lmb presented here does not provide any clues regarding the interaction of Lmb with laminin, the data presented here are valuable for the future determination of two mechanisms: Lmb–laminin binding and putative Lmb Zn^{2+} transport. This leaves us with an interesting question: is zinc binding relevant to laminin binding or are they two independent functions? In the case of Lbp it has been suggested that the interaction between Lbp and laminin is zinc-mediated (Linke *et al.*, 2009). Based on the structural and functional analogy of Lmb to Lbp, we presume that laminin binding of Lmb is also zinc-mediated, although experimental reports have yet to confirm this. Nature has expanded its repertoire of host-evasion mechanisms in an unusual and clever way by providing a dual role for Lmb in both adhesion and metal homeostasis. Hence, the crystal structure of Lmb will allow further investigations into the molecular basis of laminin binding by human pathogens and will provide new insights into host–pathogen interactions.

KP and PR thank the Department of Biotechnology (DBT), Government of India for financial support. PR thanks the University Grants Commission (UGC), Government of India for the fellowship.

References

Altschul, S. F., Madden, T. L., Schäffer, A. A., Zhang, J., Zhang, Z., Miller, W. & Lipman, D. J. (1997). *Nucleic Acids Res.* **25**, 3389–3402.

Banerjee, S., Wei, B. X., Bhattacharyya-Pakrasi, M., Pakrasi, H. B. & Smith, T. J. (2003). *J. Mol. Biol.* **333**, 1061–1069.

Bartels, K. S. & Klein, C. (2003). *The AUTOMAR Manual*, v.1.4. Norderstedt, Germany: MAR Research GmbH.

Beck, K., Hunter, I. & Engel, J. (1990). *FASEB J.* **4**, 148–160.

Boos, W. & Lucht, J. M. (1995). *Escherichia Coli and Salmonella: Cellular and Molecular Biology*, edited by F. C. Neidhardt, pp. 1175–1209. Washington: American Society for Microbiology.

Broughton, R. A. & Baker, C. J. (1983). *Infect. Immun.* **39**, 837–843.

Brünger, A. T., Adams, P. D., Clore, G. M., DeLano, W. L., Gros, P., Grosse-Kunstleve, R. W., Jiang, J.-S., Kuszewski, J., Nilges, M., Pannu, N. S., Read, R. J., Rice, L. M., Simonson, T. & Warren, G. L. (1998). *Acta Cryst.* D**54**, 905–921.

Chandra, B. R., Yogavel, M. & Sharma, A. (2007). *J. Mol. Biol.* **367**, 970–982.

Claverys, J. P. (2001). *Res. Microbiol.* **152**, 231–243.

Dintilhac, A., Alloing, G., Granadel, C. & Claverys, J. P. (1997). *Mol. Microbiol.* **25**, 727–739.

Emsley, P. & Cowtan, K. (2004). *Acta Cryst.* D**60**, 2126–2132.

Farley, M. M. (1995). *Drugs Aging*, **6**, 293–300.

Finney, L. A. & O'Halloran, T. V. (2003). *Science*, **300**, 931–936.

Hay, E. D. (1991). *Cell Biology of Extracellular Matrix*. New York: Plenum Press.

Holm, L., Kaariainen, S., Rosenstrom, P. & Schenkel, A. (2008). *Bioinformatics*, **24**, 2780–2781.

Hutchings, M. I., Palmer, T., Harrington, D. J. & Sutcliffe, I. C. (2008). *Trends Microbiol.* **17**, 13–21.

Kunitomo, E., Terao, Y., Okamoto, S., Rikimaru, T., Hamada, S. & Kawabata, S. (2008). *Microbes Infect.* **10**, 414–423.

Jones, A. L., Knoll, K. M. & Rubens, C. E. (2000). *Mol. Microbiol.* **37**, 1444–1455.

Lawrence, M. C., Pilling, P. A., Epa, V. C., Berry, A. M., Ogunniyi, A. D. & Paton, J. C. (1998). *Structure*, **6**, 1553–1561.

Lee, Y. H., Deka, R., Norgard, M. V., Radolf, J. D. & Hasemann, C. A. (1999). *Nature Struct. Mol. Biol.* **6**, 628–633.

Lee, Y. H., Dorwart, M. R., Hazlett, K. R. O., Deka, R. K., Norgard, M. V., Radolf, J. D. & Hasemann, C. A. (2002). *J. Bacteriol.* **184**, 2300–2304.

Li, H. & Jogl, G. (2007). *J. Mol. Biol.* **368,** 1358–1366.

Linke, C., Caradoc-Davies, T. T., Young, P. G., Proft, T. & Baker, E. N. (2009). *J. Bacteriol.* **191**, 5814–5823.

Ljungh, A. & Wadstrom, T. (1995). *Methods Enzymol.* **253**, 501–514.

Loisel, E., Jacquamet, L., Serre, L., Bauvois, C., Ferrer, J.-L., Vernet, T., Di Guilmi, A. M. & Durmort, C. (2008). *J. Mol. Biol.* **381**, 594–606.

Long, F., Vagin, A. A., Young, P. & Murshudov, G. N. (2008). *Acta Cryst.* D**64**, 125–132.

Newcomer, M. E., Lewis, B. A. & Quiocho, F. A. (1981). *J. Biol. Chem.* **256**, 13218−13222.

Pilka, E. S., Werner, J. M., Schwarz-Linek, U., Pickford, A. R., Meenan, N. A., Campbell, I. D. & Potts, J. R. (2006). *FEBS Lett.* **580**, 273–277.

Ponnuraj, K., Bowden, M. G., Davis, S., Gurusiddappa, S., Moore, D., Choe, D., Xu, Y., Hook, M. & Narayana, S. V. (2003). *Cell*, **115**, 217–228.

Ragunathan, P., Spellerberg, B. & Ponnuraj, K. (2009). *Acta Cryst.* F**65**, 492–494.

Rukhman, V., Anati, R., Melamed-Frank, M. & Adir, N. (2005). *J. Mol. Biol.* **348**, 961–969.

Rulísek, L. & Vondrásek, J. (1998). *J. Inorg. Biochem.* **71**, 115–127.

Sack, J. S., Saper, M. A. & Quiocho, F. A. (1989). *J. Mol. Biol.* **206**, 171−191.

Sharff, A. J., Rodseth, L. E., Spurlino, J. C. & Quiocho, F. A. (1992). *Biochemistry*, **31**, 10657–10663.

Shilton, B. H., Shuman, H. A. & Mowbray, S. L. (1996). *J. Mol. Biol.* **264**, 364–376.

Spellerberg, B., Rozdzinski, E., Martin, S., Weber-Heynemann, J., Schnitzler, N., Lutticken, R. & Podbielski, A. (1999). *Infect. Immun.* **67**, 871–878.

Weston, B. F., Brenot, A. & Caparon, M. G. (2009). *Infect. Immun.* **77**, 2840–2848.

Wei, B., Randich, A. M., Bhattacharyya-Pakrasi, M., Pakrasi, H. B. & Smith, T. J. (2007). *Biochemistry.* **46**, 8734–8743.

Zong, Y., Xu, Y., Liang, X., Keene, D. R., Hook, A., Gurusiddappa, S., Hook, M. & Narayana, S. V. (2005). *EMBO J.* **24**, 4224–4242.